2014 IEEE/RSJ International Conference on
Intelligent Robots and Systems (IROS 2014)
September 14-18, 2014, Chicago, IL, USA

MRI-powered Closed-loop Control for Multiple Magnetic Capsules

Alina Eqtami, Ouajdi Felfoul and Pierre E. Dupont

Abstract— **Control of multiple magnetic particles inside the human body may have many potential applications, such as drug delivery in places where conventional procedures cannot reach. A natural candidate for powering as well as tracking these magnetic particles is the MRI scanner. Although it offers the means to control the particles, it also poses difficulties: the magnetic field is applied uniformly to the group, thus making the independent control of each particle a challenging issue, while the actuation and the tracking are interleaved which can result to delays in actuation and measurement. The closed-loop control of a group of millimeter-scale particles, immersed in fluid, driven by the MRI scanner is studied in this paper. More specifically, this problem is presented in a unified manner, handling such issues as delays, constraints, as well as disturbances, and results in a robustly stable controller. We also propose a condition that effectively answers when the system should be in tracking mode versus actuation mode. In addition to theoretical results, the capability of the proposed controller is illustrated through simulation results.**

I. Introduction

Propelling millimeter scale robots inside fluid-filled body lumens has many potential applications. For example, a group of robots can be directed through the circulatory system to reach specific tissue targets. Alternately, the robots can be injected into the spinal canal and access the ventricles for drug delivery within the brain.

The issue of magnetically controlled robots for medical applications, has already received considerable attention in recent years. Developments focus on micron-scale robots, [2], [11], or nano-scale robots [8], proposed for a variety of medical applications as in [3], [8]. Instead, in this paper we are proposing millimeter-scale robots, as they offer advantages in some clinical applications where larger forces are needed and larger payloads should be carried, [6]. Moreover, MRI-based actuation imposes additional restrictions and difficulties that do not arise for systems powered by custom-made coils. Only a few papers have appeared that are employing clinical MRI scanners, as in [6], [10].

The topic of magnetically controlling individual robots has gained much attention, [1], [6], whereas very few results have been presented for controlling groups of magnetic robots. The design of a multi-particle formulation has considerable advantages as it can widen the medical applications that already have been proposed for a single magnetic particle. For example, delivery of drugs in multiple locations over a sustained period of time, as well as the linear increase of the overall payload that particles can deliver.

A. Eqtami, O. Felfoul and P.E. Dupont are with with Cardiac Surgery, Boston Children's Hospital, Harvard Medical School, 02115 Boston, Massachusetts. {first name. last name@childrens.harvard.edu}

Even though multi-particle magnetic control sounds appealing, there are significant challenges induced by the use of the MRI scanner. Inside the MRI bore, the same magnetic field is applied to each particle of the group. This problem can be formulated as an underactuated system with multiple states that should be controlled by one control input. A viable option is to exploit the different dynamics of each particle, thus differentiating the movement of each particle of the group. This approach has been considered in [4] for magnetic micro-robots on a planar surface, as well as in [9].

In [9], a motion planning scheme for multiple millimeter-scale capsules has been presented. The authors consider constant magnitude pulse-based gradients with different pulse widths selected to result in independent control of the position of each capsule. This motion planning scheme can achieve control of a group of particles, however, it is slow, as the particles are allowed time to come to rest after each pulse and, furthermore, it is an open-loop control scheme that can be proven inefficient in the presence of uncertainties in the systems' parameters, or in the presence of disturbances.

The problem addressed here is the independent control and stabilization of multiple magnetic spheres, of millimeter scale, swimming freely in a fluid, inside a standard clinical MRI scanner. The MRI scanner is employed both for actuation purposes and tracking, i.e. as a sensor that provides feedback. The actuation and the tracking periods are not simultaneous, but rather are interleaved. This imposes another restriction in controlling magnetic particles inside the MRI scanner, since, unlike standard closed-loop control where actuation and feedback are assumed available at each sampling instant, this is not the case with the MRI. The contribution of this paper is to derive a closed-loop control framework for the system of multiple magnetic capsules, taking into account all the restrictions of this platform. Thus, we derive a Nonlinear Model Predictive control (abbr. NMPC) scheme for the underactuated system that is affected by disturbances induced by the environment, [5]. We provide stability and robustness results for the closed-loop system. We also present a novel framework for optimal switching between actuation and tracking through the MRI, preserving the stability of the system. With the proposed framework, the appropriate gradients (input trajectory) as well as the actuation period, are decided by the controller.

The remainder of the paper is organized as follows. In Section II, the system under consideration is presented. The modeling of two ferromagnetic bodies immersed into a water tank inside an MRI, is provided first. Then a closed-loop controller is presented that is proven to be able to stabilize both ferrous capsules into their desired positions. Section

978-1-4799-6933-3/14/$31.00 ©2014 IEEE

III provides an insight on the sequences for the magnetic gradients that are used either for tracking or actuation and poses the practical question of when to track and when to actuate. Furthermore, a solution for optimal switching is provided that accounts for measurement delays as well as disturbances. Finally, in Section V some simulation examples are given and Section VI summarizes the results of this paper and indicates future research endeavors.

II. Control of Two Magnetic Capsules

Inside the MRI scanner, a uniform central field $\vec{\mathbf{B}}_0$ is present. The field $\vec{\mathbf{B}}_0$ is directed along the axis of symmetry of the bore. Placing a ferromagnetic body results in saturated magnetization $\vec{\mathbf{M}}_s$ due to this magnetic field. Moreover, the presence of gradient coils in the MRI generate a magnetic field $\vec{\mathbf{B}}_g$ along the **z**-direction. The magnitude of the magnetic field $\vec{\mathbf{B}}_g$ along the **z**-direction can be linearly modified along any direction in **xyz**-coordinates by the gradients coils and so generate a gradient field along any arbitrary direction in space.

Due to the presence of the magnetic fields, there are magnetic forces $\vec{\mathbf{F}}$ that are applied to the volume V of the ferromagnetic body and are given by:

$$\vec{\mathbf{F}} = V(\vec{\mathbf{M}}_s \nabla)\vec{\mathbf{B}}$$

where $\vec{\mathbf{B}} = \vec{\mathbf{B}}_0 + \vec{\mathbf{B}}_g$. More specifically the **xyz**-components of the force $\vec{\mathbf{F}}$ are given by:

$$[F_x,\, F_y,\, F_z]^\top = V M_{sz}[\frac{\partial B_{gz}}{\partial x},\, \frac{\partial B_{gz}}{\partial y},\, \frac{\partial B_{gz}}{\partial z}]^\top \quad (1)$$

where it was assumed that $M_{sx}, M_{sy} \ll M_{sz}$. Notice, that the magnetic fields apply also a magnetic torque $\vec{\mathbf{T}}$ that tends to rotate the ferromagnetic body as to align with the direction of the external field $\vec{\mathbf{B}}_0$. However, $\vec{\mathbf{B}}_0$ is fixed and cannot be controlled, thus, the torque is not considered here.

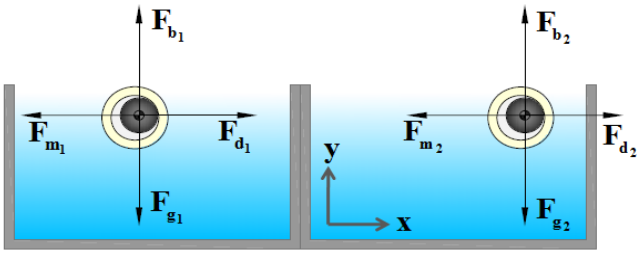

Fig. 1. Two encapsulated ferromagnetic particles, immersed into different water tanks, i.e, no interaction between them is accounted.

In this paper, we assume two encapsulated ferromagnetic spheres are immersed in water tanks. The tanks are inside the MRI bore and the goal is to control these capsules so as to move in a stable manner from their initial positions to goal positions. We assume that no dipole-dipole interaction can occur between them, i.e., the magnetic particles are sufficiently apart, [9]. Notice that, we assume two particles in order to facilitate the analysis to be more transparent. However, this analysis can be straightforwardly be applied for multiple capsules.

Since the magnetic spheres are contained inside hollow capsules, they experience buoyancy forces, $\vec{\mathbf{F}}_{b_1}$, $\vec{\mathbf{F}}_{b_2}$, that counteract the gravitational forces, $\vec{\mathbf{F}}_{g_1}$, $\vec{\mathbf{F}}_{g_2}$, along the **y**-axis, as depicted in Fig.1. Furthermore, along the **x**-axis, the magnetic forces are opposed by drag forces, $\vec{\mathbf{F}}_{d_1}$ and $\vec{\mathbf{F}}_{d_2}$. The drag force is given by: $\vec{\mathbf{F}}_d = 1/2\eta C_d A \upsilon^2$, where η is the density of the water, C_d is a drag coefficient parameter, A is the frontal area of the capsule and finally, υ is the capsule's velocity.

A. Mathematical Modeling

The equations of motion for the two magnetic particles are given by:

$$m_1\vec{\mathbf{a}}_1 = \vec{\mathbf{F}}_{d1} + \vec{\mathbf{F}}_{m1}$$
$$m_2\vec{\mathbf{a}}_2 = \vec{\mathbf{F}}_{d2} + \vec{\mathbf{F}}_{m2}$$

where m_1, m_2 are the mass of each capsule and $\vec{\mathbf{a}}_1$, $\vec{\mathbf{a}}_2$ are the **xyz**-components of acceleration for each particle. Assume that the two capsules are allowed to move only along the **x**-axis. The equation of motion for the two particles along the **x**-axis can be obtained as follows:

$$\ddot{\chi}_1 = -b_1\dot{\chi}_1^2 sign(\chi_1) + g_1\nu \quad (2a)$$
$$\ddot{\chi}_2 = -b_2\dot{\chi}_2^2 sign(\chi_2) + g_2\nu \quad (2b)$$

where $g_i \triangleq \frac{V_i M_{sz}}{m_i}$ and $b_i \triangleq \frac{\pi\eta C_{d_i} A_i}{2m_i}$ with $i = 1, 2$. The gradient $\nu \triangleq \frac{\vartheta B_{gz}}{\vartheta x}$ is the control input of the system.

Equation (2a)-(2b) can be written in stack vector form as follows:

$$\begin{bmatrix}\dot{x}_1\\ \dot{x}_2\\ \dot{x}_3\\ \dot{x}_4\end{bmatrix} = \begin{bmatrix}x_2\\ -b_1 x_2^2 sign(x_2)\\ x_4\\ -b_2 x_4^2 sign(x_4)\end{bmatrix} + \begin{bmatrix}0\\ g_1\\ 0\\ g_2\end{bmatrix}\nu \quad (3)$$

where $[x_1, x_2, x_3, x_4] \triangleq [\chi_1, \dot{\chi}_1, \chi_2, \dot{\chi}_2]$, with x_1, x_2 and x_3, x_4 to be the position and the velocity for particle 1 and particle 2, respectively.

Thus, we have a continuous-time nonlinear under-actuated system, subject to input and state constraints. The system can be re-written in the general form:

$$\dot{\hat{\mathbf{x}}} = f(\hat{\mathbf{x}}, \mathbf{u}) \quad (4)$$

where $\hat{\mathbf{x}} \triangleq [x_1, x_2, x_3, x_4]^\top$. System (4) is considered to be the "nominal" system and for now, we assume that there exist no uncertainties and/or disturbances. This assumption will be relaxed later in the paper. Assume now the compact set $\mathbf{x} \in \mathbb{X}$, where $\mathbb{X} = \{\mathbf{x} \in \mathbb{R}^4 \mid |x_1| \leq \alpha_1, |x_2| \leq \alpha_2, |x_3| \leq \alpha_3, |x_4| \leq \alpha_4\}$, with $\alpha_1, \ldots, \alpha_4 \in \mathbb{R}_+$. Also, assume that $\mathbf{u} \in \mathbb{U}$, where $\mathbb{U} = \{\mathbf{u} \in \mathbb{R}^1 \mid ||\mathbf{u}|| \leq \bar{u}\}$, with $\bar{u} \in \mathbb{R}_+$. The nominal system (4) is Lipschitz continuous in $\mathbb{X}$, with Lipschitz constant $L_f = \max\{1, 2b_1\alpha_2, 2b_2\alpha_4\}$. This can easily be verified, taking the ∞-norm of the Jacobian of system (4) and proving that is bounded by L_f in $\mathbb{X}$.

We need to find a control law that can drive the two particles from an initial position to a desired final position while respecting the constraints. Notice, that controlling particles inside the human body will have restrictions, thus

fulfilment of the constraints is of paramount importance. A control methodology that allows explicit incorporation of input and state constraints is Model Predictive Control and this is the approach that will be employed here.

B. Constrained Model Predictive Control

The NMPC control problem is essentially an open-loop optimal control problem that is solved at discrete-time instants k_i based on the current state information $x(k_i)$. Two successive instants are k_i and k_{i+1}, with $k_i \leq k_{i+1}$ and $k_i \to \infty$ for $i \to \infty$. Furthermore, we have: $\inf_{i\in\mathbb{N}}(k_{i+1} - k_i) \leq k_{i+1} - k_i \leq \sup_{i\in\mathbb{N}}(k_{i+1} - k_i)$, i.e., there exists an upper and lower bound on the inter-sampling period. Notice that the lower bound is imposed by technical demands, as for example how fast the MRI software can perform the tracking. Specific details on the time constraints imposed by the MRI tracking will be fully explained later. Hereafter, this lower bound is going to be considered to be the sampling period. The upper bound is going to be computed in the next sections of the paper.

The NMPC consists in solving a finite-horizon, open-loop optimal control problem, based on the actual state of the plant $\mathbf{x}(k_i)$, at time k_i. The solution is a control trajectory $\mathbf{u}(t)$, for $t \in [k_i, k_i + T]$, where T is the prediction horizon. The Optimal Control Problem (abbr. OCP) of the NMPC is given as $\min_{\mathbf{u}(\cdot)} J(\mathbf{u}(\cdot), x(k_i))$:

$$\min_{\mathbf{u}(\cdot)} \int_{k_i}^{k_i+T} L(\hat{\mathbf{x}}(s), \mathbf{u}(s))\ \mathrm{d}\, s + V(\hat{\mathbf{x}}(k_i + T)), \tag{5a}$$

$$\text{s.t.} \quad \dot{\hat{\mathbf{x}}} = f(\hat{\mathbf{x}}(t), \mathbf{u}(t)), \qquad \hat{\mathbf{x}}(k_i) = \mathbf{x}(k_i), \tag{5b}$$

$$\mathbf{u}(t) \in \mathbb{U}, \tag{5c}$$

$$\hat{\mathbf{x}}(t) \in \mathbb{X} \qquad t \in [k_i, k_i + T], \tag{5d}$$

$$\hat{\mathbf{x}}(k_i + T_p) \in \mathbb{X}_t, \tag{5e}$$

where the design parameters $L(\cdot,\cdot)$ and $V(\cdot)$ are the running and terminal costs functions, respectively.

Assume now that the terminal cost $V(\mathbf{x})$ as well as the cost function $L(\mathbf{x}, \mathbf{u})$, are quadratic of the form $V(\mathbf{x}) = \mathbf{x}^\top P \mathbf{x}$ and $L(\mathbf{x}, \mathbf{u}) = \mathbf{x}^\top Q \mathbf{x} + \mathbf{u}^\top R \mathbf{u}$, respectively. More specifically we set P and Q to be positive definite diagonal matrices in $\mathbb{R}^{4\times4}$ and $R \in \mathbb{R}_+$. Moreover it can easily be shown that $L(0, 0) = 0$ and that it is also positive definite matrix. More specifically since $\mathbb{X}$ and $\mathbb{U}$ are bounded, it can be concluded that the stage cost $L(\mathbf{x}, \mathbf{u})$ and that the terminal cost $V(\mathbf{x})$ are Lipschitz continuous in $\mathbb{X} \times \mathbb{U}$ and $\mathbb{X}$, with a Lipschitz constants L_l and L_v, respectively. The solution of the optimal control problem is denoted as $\mathbf{u}^\star(\cdot; x(k_i))$. It defines the open-loop control input that is applied to the system until the next sampling instant k_{i+1}. It can be shown that:

$$\mathbf{u}(t, x(k_i)) = \mathbf{u}^\star(t, x(k_i)) \qquad \forall\, t \in [k_i, k_{i+1}) \tag{6}$$

In the standard closed-loop approach, the control (6) is recalculated at predefined sampling instants, where a new state measurement is available and the procedure is repeated again, until the systems' state has reached the desired terminal set $\mathbb{X}_t$. Assume also:

Assumption 1: There exists a local stabilizing controller $h(\mathbf{x}(t))$ for all $\mathbf{x} \in \mathbb{X}_t$. The associated Lyapunov function $V(\cdot)$ has the following properties: $\frac{\partial V}{\partial x} f(\mathbf{x}(t), h(\mathbf{x}(t))) + L(\mathbf{x}(t), h(\mathbf{x}(t))) \leq 0$, for all $\mathbf{x} \in \mathbb{X}_t$.

System (2a)-(2b) is a second order nonlinear system with drift. Furthermore, the driftless system is not controllable. Such systems are infamous for being extremely difficult to derive controllability. In this paper, however, we do not assume an explicit controllability assumption, but instead derive stability under the assumption of initial feasibility of the optimal control problem.

We are now ready to derive the stability of the overall framework: The proof of stability of a system under a predictive controller consists in guaranteeing (i) the feasibility property and (ii) the convergence property of the closed-loop system. We begin by showing that initial feasibility implies feasibility afterwards. Consider two successive sampling instants: k_i and k_{i+1}. A feasible control trajectory is given as:

$$\tilde{u}(t, \mathbf{x}(k_{i+1})) = \tag{7}$$
$$\begin{cases} u^\star(t, \mathbf{x}(k_i)) & \forall t \in [k_{i+1}, k_i + T] \\ h(\hat{\mathbf{x}}(k_i + T, u^\star(\cdot), \mathbf{x}(k_i))) & \forall t \in [k_i + T, k_{i+1} + T] \end{cases}$$

where $u^\star(\cdot, \mathbf{x}(k_i))$ is the optimal solution of the OCP at time instant k_i. The control trajectory $u^\star(\cdot, \mathbf{x}(k_i))$ belongs to $\mathbb{U}$ and $h(\mathbf{x}) \in \mathbb{U}$ for all $\mathbf{x} \in \mathbb{X}_t$. It follows that $\tilde{u}(\tau, \mathbf{x}(k_{i+1})) \in \mathbb{U}$ for all $t \in [k_{i+1}, k_{i+1} + T]$. Also, since we do not assume disturbances: $\mathbf{x}(k_{i+1}) = \hat{\mathbf{x}}(k_{i+1}, u^\star(t, \mathbf{x}(k_i)), \mathbf{x}(k_i)) \in \mathbb{X}$. Furthermore, $\hat{\mathbf{x}}(k_i + T) = \hat{\mathbf{x}}(k_i + T, u^\star(t, \mathbf{x}(k_i)), \mathbf{x}(k_i)) \in \mathbb{X}_t$. From Assumption 1 there exists $h(t)$ that renders $\mathbb{X}_t$ invariant. Thus, for the time instant k_{i+1}, the input (7) is feasible, hence feasibility at time k_i implies feasibility at k_{i+1}. Finally, we can conclude that the if the problem is feasible for $t = 0$, then it is feasible for all $t \geq 0$. Now, we take as a Lyapunov function candidate the optimal cost $J^\star(\mathbf{x})$ from (5a), i.e., $J^\star(\mathbf{x}) \triangleq J(u^\star(\cdot, \mathbf{x}), \mathbf{x})$. We will prove that this Lyapunov function is strictly decreasing for all $\mathbf{x} \neq 0$ between two successive sampling instants k_i and k_{i+1}:

Take two successive arbitrary time instants k_i and k_{i+1} and assume that there is some $\tau \in (0, k_{i+1} - k_1]$. We have: $J^\star(u^\star, \mathbf{x}(k_i)) = \int_{k_i}^{k_i+T} L(\hat{\mathbf{x}}(s, u^\star, \mathbf{x}(k_i)), u^\star)\ \mathrm{d}\, s$ $+\ V(\hat{\mathbf{x}}(k_i + T, u^\star, \mathbf{x}(k_i)))$ and $J(\tilde{u}, \mathbf{x}(k_i + \tau)) = \int_{k_i+\tau}^{k_i+\tau+T} L(\hat{\mathbf{x}}(s, \tilde{u}, \mathbf{x}(k_i + \tau)), \tilde{u})\ \mathrm{d}\, s$ $+ V(\hat{\mathbf{x}}(k_i + \tau + T, \tilde{u}, \mathbf{x}(k_i + \tau)))$. With some manipulation, this yields:

$$J(\tilde{u}, \mathbf{x}(k_i + \tau)) - J^\star(u^\star \mathbf{x}(k_i)) \leq$$
$$- \int_{k_i}^{k_i+\tau} L(\hat{\mathbf{x}}(s, u^\star, \mathbf{x}(k_i)), u^\star)\ \mathrm{d}\, s \tag{8}$$

The cost $L(\cdot,\cdot)$ is designed to be positive definite. Notice that $J(\tilde{u}, \mathbf{x}(k_i + \tau))$ is a "feasible" cost since it is computed based on a feasible control input (7). From the optimality of the solution it can be obtained that: $J^\star(u^\star, \mathbf{x}(k_i + \tau)) \leq J(\tilde{u}, \mathbf{x}(k_i + \tau))$. Hence, (8) results that the Lyapunov function

is strictly decreasing, except $\mathbf{x}(k_i) \neq 0$. Since this holds for arbitrary time instants k_i, will hold for all sampling instants. Thus, we have proven the convergence of the solutions of the closed-loop system (4)-(6) to zero: $\mathbf{x} \to 0$ for $t \to \infty$.

III. Optimal Switching between Actuation and Tracking

The time period that the MRI gradient sequences require for acquiring data, e.g., acquiring particle positions, is lower bounded by constraints that are discussed below. This bound is naturally considered constant. The actuation period, however, can be decided by the user. The decision is usually based on a compromise, because a large actuation period may result in problems similar to open-loop control, while a very small actuation period results in a small duty cycle. Rather than employ an ad-hoc criterion, the approach proposed here allows the controller to decide the duration of actuation based on system state measurements.

A. Problem Formulation

An MRI sequence performing alternating tracking and actuation of two capsules is depicted in Fig. 2. The tracking sequence consists of acquiring a $1D$ projection using Radio-Frequency (abbr. RF) excitation followed by a readout gradient. The duration of the tracking sequence depends on the imaging parameters such as Field Of View (abbr. F.O.V.) and resolution, and can be made < 10msec. Beside tracking sequence length, there exist other delays, such as the time periods required for computing capsule position and computing the control law. Furthermore, there is also a delay required for sending and applying the next control inputs. These delays are empirically estimated to range between 10 and 30msec depending on the level of computation needed and the processor used. These delays determine the minimum time between consecutive tracking phases, which is also limited by physical constraints. In fact, after spins are excited, they need some time to return to equilibrium. This period depends on their intrinsic T_1 and T_2 relaxation times, which are tissue dependent. Notice also, that if very fast tracking refresh rates are used, signal loss can occur, causing a decrease in the S.N.R. (abbr. Signal to Noise Ratio). The low-order system described here is tractable with existing computing power. Position tracking of the spheres (even for $2D$) takes about 17msec, and so an overall of 20msec is assumed. This means that the system receives the value of its state measurement with a delay of Δ-time period, where $\Delta = 20$msec=const.$\in \mathbb{R}_+$. We should find a control law closely related to (6), that is applied for some time period, accounting for measurement delay, and rendering the overall closed-loop system stable:

$$\mathbf{u}(t, x(k_i)) = \mathbf{u}^\star(t, x(k_i)) \qquad \forall\, t \in [k_i, k_{i+1} - \Delta) \tag{9}$$

We will treat this delay as a disturbance. Moreover, the environment induces other forms of disturbances, due to the presence of water, that may alter the state trajectory of the spheres. Assume now that the nominal system (4), is affected by additive and bounded disturbances:

$$\dot{\mathbf{x}} = f(\mathbf{x}, \mathbf{u}) + \mathbf{d}(t) \tag{10}$$

where $\mathbf{d}(t)$ is the overall disturbance term comprising the disturbance $\mathbf{d}_1(t)$, due to computational/tracking delay and the disturbance $\mathbf{d}_2(t)$, induced from the environment. The latter is assumed to be bounded.

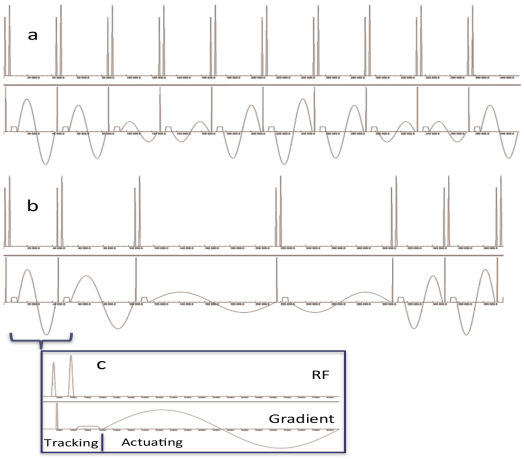

Fig. 2. (a) Constant sampling. The diagrams depict the tracking sequences and the actuation sequences. (b) Variable sampling. Optimal switching between actuation and tracking. The diagrams depict the tracking sequences and the actuation sequences. (c) A detailed view of one period of actuation and tracking.

Note that the magnitude of the control input during tracking is very close to zero, i.e., $\mathbf{u}(t) \simeq 0$ for some $t \in \mathbb{R}_+$. Using the nominal system (4), trajectory deviation due to tracking can be assessed during the time period Δ. For an arbitrary time-step k_i and a slight violation of the notation, it can be shown that:

$$||\hat{\mathbf{x}}(k_i + \Delta) - \hat{\mathbf{x}}(k_i)|| \leq \int_{k_i}^{k_i+\Delta} ||f(\hat{\mathbf{x}}(s), 0)||\, \mathrm{d}\, s \leq L_f \Delta$$

and thus, the deviation is bounded. Hence, we can assume the following: $||\mathbf{d}(t)|| \leq \gamma$ with $\gamma \in \mathbb{R}_+$.

B. Optimal Switching

In order to proceed to the subsequent analysis, some definitions and preliminary results are presented first. Assume that at an arbitrary time instant k_i, a measurement of the system's state is available. The predicted state of the nominal system (4) at an arbitrary time instant $k_i + t$ with $t \in \mathbb{R}_+$, is given as: $\hat{\mathbf{x}}(k_i + t, u(\cdot), \mathbf{x}(k_i))$. It holds that $\hat{\mathbf{x}}(k_i, u(\cdot), x(k_i)) \equiv x(k_i)$, i.e., at the time step of measurement, no divergence is assumed. However, the actual system (10), has a different trajectory than the predicted one, due to the presence of disturbances, i.e., the actual trajectory of the system for the same input trajectory will be denoted as: $\mathbf{x}(k_i + t, u(\cdot), \mathbf{x}(k_i))$. Thus, we are ready now to find a bound on the trajectory divergence between the actual system and the nominal system:

Lemma 1: The difference between the actual state $\mathbf{x}(k_i + t)$ at time $k_i + t$ and the predicted state at the same time

under the same control law $u(k_i+t, \mathbf{x}(k_i))$, with $0 \leq t \leq T$, starting at the same initial state $\mathbf{x}(k_i)$, can be shown to be upper bounded by:

$$||\mathbf{x}(k_i+t) - \hat{\mathbf{x}}(k_i+t, u(\cdot), \mathbf{x}(k_i))|| \leq \beta \cdot t \qquad (11)$$

for all $t \in [0, T]$, with $\beta \triangleq L_f((2\alpha_1)^2 + (2\alpha_2)^2 + (2\alpha_3)^2 + (2\alpha_4)^2)^{1/2} + \gamma$.

Proof: Using the Euclidian norm and the triangular inequality for system (4) and system (10), we get:

$$\begin{aligned}
&||\mathbf{x}(k_i+t) - \hat{\mathbf{x}}(k_i+t)|| = ||\mathbf{x}(k_i) + \int_{k_i}^{k_i+t} f(\mathbf{x}(s), u(\cdot))\ \mathrm{d}\, s \\
&+ \int_{k_i}^{k_i+t} d(s)\ \mathrm{d}\, s - \mathbf{x}(k_i) - \int_{k_i}^{k_i+t} f(\hat{\mathbf{x}}(s), u(\cdot))\ \mathrm{d}\, s|| \\
&\leq || \int_{k_i}^{k_i+t} f((\mathbf{x}(s), u(\cdot)) - f(\hat{\mathbf{x}}(s), u(\cdot))\ \mathrm{d}\, s|| \\
&+ || \int_{k_i}^{k_i+t} d(s)\ \mathrm{d}\, s|| \leq \int_{k_i}^{k_i+t} L_f ||\hat{\mathbf{x}}(\cdot) - \mathbf{x}(\cdot)||\ \mathrm{d}\, s \\
&+ \int_{k_i}^{k_i+t} ||d(s)||\ \mathrm{d}\, s + \leq \beta \cdot t
\end{aligned}$$

■

In order to find a controller that can stably drive the actual system (10) to a desired position using (9), a Model Predictive framework similar to (6) as given by (5a)-(5e) will be used. However, some modifications are necessary in order to address the divergence between the actual state trajectory of system (10) and the predicted state trajectory of the nominal system (4) as was given in Lemma 1. In this case, we must ensure that the state constraints will be fulfilled throughout the prediction horizon, despite the presence of the disturbances. In order to account for that, we replace the state constraint set $\mathbb{X}$ with the restricted constraint set $\mathbb{X}_{t-k_i}$ into (5d), with $\mathbb{X}_{t-k_i} \subseteq \mathbb{X}$ and the terminal state set $\mathbb{X}_t$ by $\mathbb{X}_f$ such that $\forall \mathbf{x} \in \mathbb{X}_t, f(\mathbf{x}, h(\cdot)) \in \mathbb{X}_f$. More details on this constraint tightening technique are given in [7].

We are now ready to prove convergence of the closed-loop system (10)-(9) similar to the stability proof of the nominal system, (4)-(6). Later, we are going to employ this result to find the condition for switching between actuation and tracking. For simplicity, we are using the following notation: For some arbitrary $\tau \in \mathbb{R}_+$, for some time instant where a measurement is available $k_i \in \mathbb{R}_+$ and some $t \in (k_i, k_i+T]$, we denote as $J^\star(k_i) \equiv J^\star(u^\star(\cdot), x(k_i))$, $J(t) \equiv J(\tilde{u}(\cdot), \mathbf{x}(t))$, $\tilde{\mathbf{x}}(\tau) \equiv \tilde{\mathbf{x}}(\tau, \tilde{u}(\tau, \mathbf{x}(t)), \mathbf{x}(t))$, $\hat{\mathbf{x}}(\tau) \equiv \hat{\mathbf{x}}(\tau, u^\star(\tau, \mathbf{x}(k_i)), \mathbf{x}(k_i))$ and the control inputs $\tilde{u}(\tau) \equiv \tilde{u}(\tau, \mathbf{x}(t))$ and $u^\star(\tau) \equiv u^\star(\tau, \mathbf{x}(k_i))$.

The difference between the costs is given by:

$$\begin{aligned}
&J(t) - J^\star(k_i) = \\
&\int_t^{t+T} L(\tilde{\mathbf{x}}(s), \tilde{u}(s))\ \mathrm{d}\, s + V(\tilde{\mathbf{x}}(t+T)) \\
&- \int_{k_i}^{k_i+T} L(\hat{\mathbf{x}}(s), u^\star(s))\ \mathrm{d}\, s - V(\hat{\mathbf{x}}(k_i+T)) \\
&= \int_t^{k_i+T} L(\tilde{\mathbf{x}}(s), \tilde{u}(s))\ \mathrm{d}\, s + V(\tilde{\mathbf{x}}(t+T)) \\
&+ \int_{k_i+T}^{t+T} L(\tilde{\mathbf{x}}(s), \tilde{u}(s))\ \mathrm{d}\, s - \int_{k_i}^{t} L(\hat{\mathbf{x}}(s), u^\star(s))\ \mathrm{d}\, s \\
&- \int_t^{k_i+T} L(\hat{\mathbf{x}}(s), u^\star(s))\ \mathrm{d}\, s - V(\hat{\mathbf{x}}(k_i+T)) \qquad (12)
\end{aligned}$$

From (7) we get: $\tilde{u}(\tau) \equiv u^\star$ for $\tau \in [t, k_i+T]$, thus we obtain the following:

$$\begin{aligned}
&\int_t^{k_i+T} L(\tilde{\mathbf{x}}(s), \tilde{u}(s))\ \mathrm{d}\, s - \int_t^{k_i+T} L(\hat{\mathbf{x}}(s), u^\star(s))\ \mathrm{d}\, s \\
&\leq \int_t^{k_i+T} ||L(\tilde{\mathbf{x}}(s), u^\star(\cdot)) - L(\hat{\mathbf{x}}(s), u^\star(\cdot))||\ \mathrm{d}\, s \leq \\
&L_l \int_t^{k_i+T} ||\tilde{\mathbf{x}}(s) - \hat{\mathbf{x}}(s)||\ \mathrm{d}\, s \leq L_l \int_t^{k_i+T} \beta \cdot (t-k_i)\ \mathrm{d}\, s \\
&= L_l \beta \cdot (t-t_i)(k_i+T-t) \qquad (13)
\end{aligned}$$

which is lower bounded by zero from the definition of t. Integrating the inequality from Assumption 1 for $\tau \in [k_i+T, t+T]$ results in the following:

$$\begin{aligned}
&\int_{k_i+T}^{t+T} L(\tilde{\mathbf{x}}(s), \tilde{u}(s))\ \mathrm{d}\, s + V(\tilde{\mathbf{x}}(t+T)) \\
&- V(\hat{\mathbf{x}}(k_i+T)) - V(\tilde{\mathbf{x}}(k_i+T)) + V(\tilde{\mathbf{x}}(k_i+T)) \\
&\leq V(\tilde{\mathbf{x}}(k_i+T)) - V(\hat{\mathbf{x}}(k_i+T)) \\
&\leq L_v ||\tilde{\mathbf{x}}(k_i+T) - \hat{\mathbf{x}}(k_i+T)|| \\
&\leq L_v \beta \cdot (t-k_i) \geq 0 \qquad (14)
\end{aligned}$$

Since function $L(\cdot, \cdot)$ is positive definite, it can be concluded that:

$$\int_{k_i}^{t} L(\hat{\mathbf{x}}(s), u^\star(s))\ \mathrm{d}\, s \geq 0 \qquad (15)$$

Substituting (15), (14) and (13) into (12), results in:

$$\begin{aligned}
&J^\star(t) - J^\star(k_i) \leq J(t) - J^\star(k_i) \\
&\leq L_l \beta \cdot (t-t_i)(k_i+T-t) + L_v \beta \cdot (t-k_i) \\
&- \int_{k_i}^{t} L(\hat{\mathbf{x}}(s), u^\star(s))\ \mathrm{d}\, s \qquad (16)
\end{aligned}$$

The value function $J^\star(\cdot)$ has been proven to be decreasing, thus the closed-loop system converges to a compact set $\mathbb{X}_t$, where it is ultimately bounded. It should be noted that in the presence of disturbances only boundedness results can be acquired.

Consider that at time k_i the controller receives a measurement $\mathbf{x}(k_i)$. We are ready now to derive sufficient conditions for switching between actuation and tracking. From (16) we can see that $J^\star(\cdot)$ behaves as an Input-to-State Lyapunov function. The next control update time t should be such that the closed-loop system does not lose any of its desired properties. Thus, we still need the Lyapunov function $J^\star(\cdot)$ to be decreasing, which will preserve the convergence of the

closed-loop system. The time instant t should be such that

$$L_l\beta\cdot(t-t_i)(k_i+T-t)+L_v\beta\cdot(t-k_i)$$
$$\leq\sigma\int_{k_i}^{t}L(\hat{\mathbf{x}}(s),u^\star(s))\,\mathrm{d}\,s \quad (17)$$

with $0<\sigma<1$. Plugging in (17) to (16) we get

$$J^\star(t)-J^\star(k_i)\leq(\sigma-1)\cdot\int_{k_i}^{t}L(\hat{\mathbf{x}}(s),u^\star(s))\,\mathrm{d}\,s \quad (18)$$

This suggests that provided $\sigma<1$, the convergence property is still guaranteed. Thus, the next control update time should be computed when condition (17) is violated. Notice that the time t can be found analytically beforehand at time k_i. Thus, at a time k_i when a measurement is available, we are able to predict when a new measurement should be acquired again. This results in a robustly stable framework, having taken into account all the disturbances and the delays in the measurement.

IV. Simulation Examples

The aim of this section is to show the efficacy of the proposed controller to perform stabilization of two magnetic capsules to their desired positions. The capsules are modeled as in (2a)-(2b), i.e., to be two nonlinear systems with drift, with the same form but different parameters, so as to achieve differentiation in their position trajectories. In particular, one ferromagnetic particle is selected to be twice the radius of the other. All parameters used in the simulations are listed in Table I.

TABLE I
Model Parameters

Parameters	Value
Radius of ferrous sphere 1 $[m]$	0.0015
Radius of ferrous sphere 2 $[m]$	0.0030
Radius of capsules $[m]$	0.0045
Density of ferrous spheres $[Kg/m^3]$	7850
Magnetization of ferrous spheres $[Am^{-1}]$	$1.36\cdot10^6$
Dynamic viscosity of the fluid $[Pas]$	$1.00\cdot10^{-3}$
Density of the fluid $[Kg/m^3]$	$1.00\cdot10^3$
Q-matrix (Diagonal)	$[0.02, 0.001, 0.02, 0.001]$
R-matrix	$1.00\cdot10^{-5}$
P-matrix	$10^{-3}\cdot Q$
Sampling period $[sec]$	0.02
Gradient amplitude $[T/m]$	±0.04
Prediction horizon $[sec]$	$10\cdot0.02$
Initial position of the capsules	$[0,0,0,0]^\top$

The initial position of the capsules for all simulations is $\mathbf{x}_{\text{initial}}=[0,\,0,\,0,\,0]^\top$. It is assumed here that the particles are sufficiently separated in the other coordinate directions so as to avoid interaction effects. Two case studies were considered in order to depict the efficacy of the proposed controller. In the first example, the goal is to drive the capsules from their initial position to a desired position $\mathbf{x}_A=[2,\,0,\,3,\,0]^\top$, i.e., to be driven to the same direction. This is depicted in Fig.3. The second goal is to move one capsule in the positive direction and the other in the negative direction, $\mathbf{x}_C=[2,\,0,\,-1,\,0]^\top$, as depicted in Fig. 4. A detailed view of the last goal is depicted in Fig. 5, where the differentiation in the motion of the capsules is illustrated. Notice, that the blue solid line represents the position of the small capsule, the red solid line represents the position of the larger capsule and the black solid line represents the control input, i.e., the magnetic gradient. From this figure we can see that in the first period, where the input is close to zero both spheres are accelerating in the negative direction. Next, a control pulse accelerates them both in the positive direction and, finally, a smaller pulse causes the smaller particle to change direction, while momentum continues to carry the larger particle in the positive direction. In this way, the controller can generate motion of the two capsules in opposite directions using a single control input. To consider

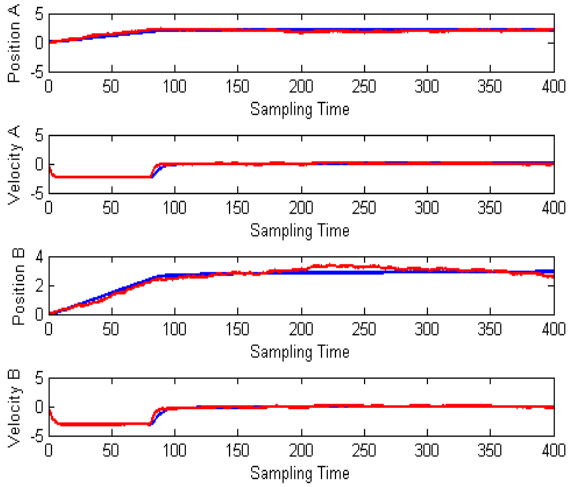

Fig. 3. Position and Velocity of the two capsules. The blue solid line the nominal system, while the red solid line represents the system affected by the disturbances. The desired position is $\mathbf{x}_A=[2,\,0,\,3,\,0]^\top$.

disturbances arising from immersion in a fluid, we also consider here additive disturbances with $||\mathbf{d}||\leq0.05$. As shown in the figures, the capsules are still stabilized in a bounded set around their desired positions. Notice, that we assumed a prediction horizon $T=10$. If a bigger prediction horizon is used, the resulting trajectory may be smoother, but at the price of higher computational time.

To evaluate our criteria for variable sampling time combined with disturbances, Fig. 6 plots capsule position versus time for the same initial conditions as Fig. 3. The system performs robustly under this framework, while the duty cycle is significantly increased as is depicted in Fig. 7, i.e., with the proposed approach, we can achieve similar performance but bigger duty cycles. Notice that, after sampling instant 70, the system has essentially reached the desired set.

V. Conclusions

This paper presents a unified control framework for a group of millimeter-scale ferrous spheres immersed into fluid, controlled through the MRI. The issues of presence of constraints, disturbances and delays are discussed and a sufficient condition that decides when the MRI should actuate and when to track is derived. The paper focuses on the

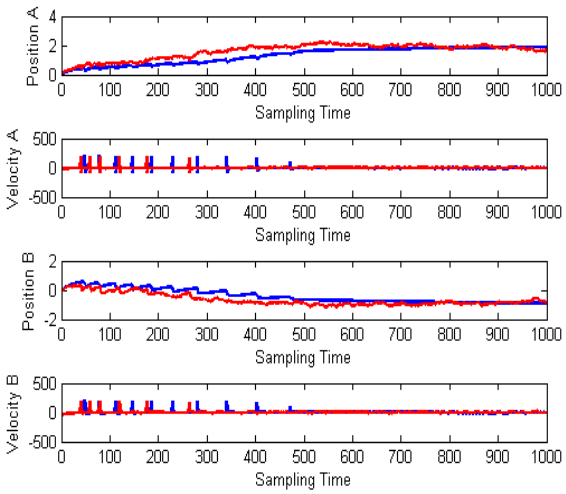

Fig. 4. Position and Velocity of the two capsules. The blue solid line represents the nominal system, while the red solid line represents the system affected by the disturbances. The desired position is $\mathbf{x}_C = [2,\ 0,\ -1,\ 0]^\top$.

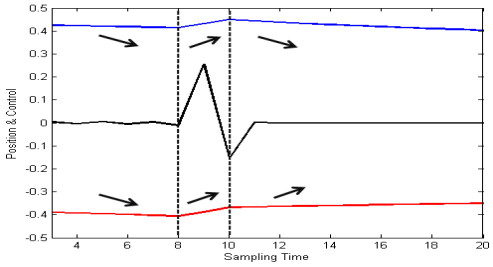

Fig. 5. Detailed view of Fig.4. The blue solid line represents the position of the small capsule, the red line represents the position of the large capsule and the black solid line represents the magnetic gradients. The desired position is $\mathbf{x}_C = [2,\ 0,\ -1,\ 0]^\top$.

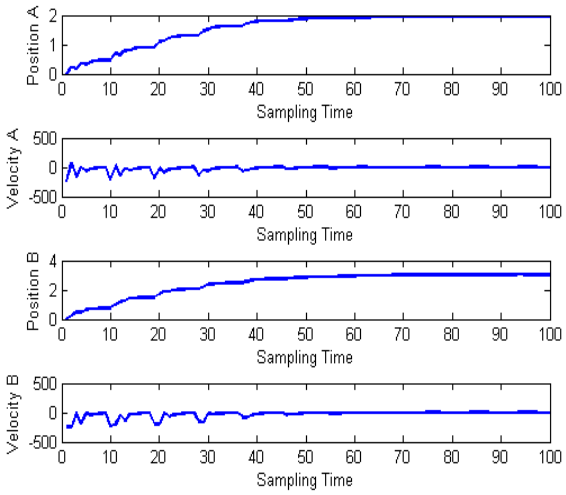

Fig. 6. Position and Velocity of the two capsules. The blue solid line represents the system affected by additive, bounded disturbances, while employing variable sampling. The desired position is $\mathbf{x}_A = [2,\ 0,\ 3,\ 0]^\top$.

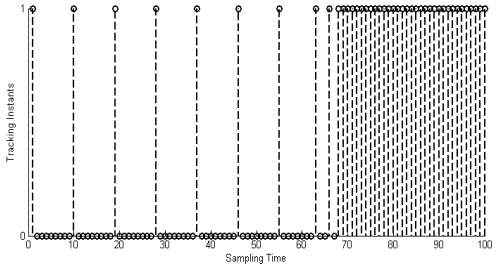

Fig. 7. Sampling instants of Fig. 6. The stems represent the tracking instances. When it is zero, the actuation mode is on.

control of two magnetic particles, however, this framework can straightforwardly be applied in multiple particles.

Current studies are focusing on experimental validation of the proposed scheme. Also, future research effort will be devoted towards addressing magnetic interactions of the capsules.

VI. Acknowledgements

This work was supported by the National Science Foundation under grant IIS-1208509 and by the Wyss Institute for Biologically Inspired Engineering.

References

[1] L. Arcese, M. Fruchard, F. Beyeler, A. Ferreira, and B.J. Nelson. Adaptive backstepping and MEMS force sensor for an MRI-guided microrobot in the vasculature. In *Robotics and Automation (ICRA), 2011 IEEE International Conference on*, pages 4121–4126, May 2011.

[2] B. Bekham and M. Sitti. Bacterial flagella-based propulsion and on/off motion control of microscale objects. *Ap. Ph. Letters*, 90(2):1–3, 2007.

[3] C. Bergeles, M.P. Kummer, B.E. Kratochvil, C. Framme, and B.J. Nelson. Steerable intravitreal inserts for drug delivery: In vitro and ex vivo mobility experiments. In *Medical Image Computing and Computer-Assisted Intervention MICCAI 2011*, volume 6891 of *Lecture Notes in Computer Science*, pages 33–40. Springer Berlin Heidelberg, 2011.

[4] E. Diller, S. Floyd, C. Pawashe, and M. Sitti. Control of multiple heterogeneous magnetic micro-robots on non specialized surfaces. *IEEE International Conference on Robotics and Automation*, pages 115 – 120, 2011.

[5] A. Eqtami, D.V. Dimarogonas, and K.J. Kyriakopoulos. Novel event-triggered strategies for model predictive controllers. *50th IEEE Conf. Decision and Control & Eur. Control Conf.*, pages 3392–3397, 2011.

[6] O. Felfoul, E. Aboussouan, A. Chanu, and S. Martel. Real-time positioning and tracking technique for endovascular unterthered microrobots propelled by MRI-gradients. *IEEE International Conference on Robotics and Automation*, pages 2693 – 2698, 2009.

[7] D. Limon Marruedo, T. Alamo, and E.F. Camacho. Input-to-state stable mpc for constrained discrete-time nonlinear systems with bounded additive uncertainties. *41st IEEE Conf. Decision and Control*, pages 4619 – 4624, 2002.

[8] P. Pouponneau, J.-C. Leroux, and S. Martel. Magnetic nanoparticles encapsulated into biodegradable microparticles steered with an upgrated magnetic resonance imaging system for tumor chemoembolization. *Biomaterial*, 30:6327–6332, 2009.

[9] P. Vartholomeos, M.R. Akhavan-Sharif, and P.E. Dupont. Motion planning for multiple millimeter-scale magnetic capsules in a fluid environment. *IEEE International Conference on Robotics and Automation (ICRA)*, pages 1927–1932, 2012.

[10] P. Vartholomeos and C. Mavroidis. Simulation platform for self-assembly structures in MRI-based nanorobotic drug delivery system. *IEEE International Conference on Robotics and Automation*, pages 5594 – 5600, 2010.

[11] K.B. Yeşin, K. Vollmers, and B.J. Nelson. Modeling and control of untethered biomicrorobots in a fluidic environment using electromagnetic fields. *Int. Journal of Robotics Research*, 25(5-6):527–536, 2006.